ACCELERATED PUBLICATION

Probing nucleotide-binding effects on backbone dynamics and folding of the nucleotide-binding domain of the sarcoplasmic/endoplasmic-reticulum Ca^{2+}-ATPase

Mona ABU-ABED*, Oscar MILLET†, David H. MacLENNAN* and Mitsuhiko IKURA‡[1]

*Banting and Best Departments of Medical Research, University of Toronto, 112 College Street, Toronto, Ontario, Canada M5G 1L6, †Department of Medical Genetics, University of Toronto, Toronto, ON, Canada M5S 1A8, and ‡Division of Molecular and Structural Biology, Ontario Cancer Institute and Department of Medical Biophysics, University of Toronto, 610 University Avenue, Toronto, Ontario, Canada M5G 2M9

In muscle cells, SERCA (sarcoplasmic/endoplasmic-reticulum Ca^{2+}-ATPase) plays a key role in restoring cytoplasmic Ca^{2+} levels to resting concentrations after transient surges caused by excitation–coupling cycles. The mechanism by which Ca^{2+} is translocated to the lumen of the ER (endoplasmic reticulum) involves major conformational rearrangements among the three cytoplasmic domains: actuator (A), nucleotide-binding (N) and phosphorylation (P) domains; and within the transmembrane Ca^{2+}-binding domain of SERCA. CD, fluorescence spectroscopy and NMR spectroscopy were used in the present study to probe the conformation and stability of the isolated N domain of SERCA (SERCA-N), in the presence and absence of AMP-PNP (adenosine 5′-[β,γ-imido]triphosphate). CD and tryptophan fluorescence spectroscopy results established that the effects of nucleotide binding were not readily manifested on the global fold and structural stability of SERCA-N. ^{15}N-backbone-relaxation experiments revealed site-specific changes in backbone dynamics that converge on the central β-sheet domain. Nucleotide binding produced diverse effects on dynamics, with enhanced mobility observed for Ile^{369}, Cys^{420}, Arg^{467}, Asp^{568}, Phe^{593} and Gly^{598}, whereas rigidifying effects were found for Ser^{383}, Leu^{419}, Thr^{484} and Thr^{532}. These results demonstrate that the overall fold and backbone motional properties of SERCA-N remained essentially the same in the presence of AMP-PNP, yet revealing evidence for internal counter-balancing effects on backbone dynamics upon binding the nucleotide, which propagate through the central β-sheet.

Key words: Ca^{2+}-ATPase, SERCA, nucleotide binding domain, NMR, relaxation, backbone dynamics.

INTRODUCTION

SERCA (sarcoplasmic/endoplasmic-Ca^{2+}-ATPase) is one of the primary cell machines that set cytosolic Ca^{2+} levels in muscle cells [1]. It functions as a pump at the SR (sarcoplasmic reticulum) or ER (endoplasmic reticulum) membrane, whereby it translocates Ca^{2+} from the cytosol into the SR/ER lumen in an ATP-dependent manner. SERCA enzymes are relatively large proteins (approx. 112 kDa) that form a phosphoprotein intermediate and undergo conformational changes during the course of ATP hydrolysis and Ca^{2+} transport. All known SERCA isoforms consist of a large cytoplasmic region composed of three subdomains anchored to the SR/ER membrane by ten transmembrane segments (TM1–TM10). The three cytosolic domains: the phosphorylation (P), nucleotide-binding (N) and actuator (A) domains, form the catalytic site. Although the N and P domains are responsible for phospho-intermediate formation, the A domain may contribute to dephosphorylation [2].

Structural studies have given ample evidence of changes in the topology of SERCA at different stages of the Ca^{2+} translocation cycle [3,4]. Structural changes in the TM segments, caused by Ca^{2+} binding, have long-range effects on the cytoplasmic domains and drive the transition between different reactive states. The details of intradomain changes occurring on the cytoplasmic side of the protein have not yet been fully characterized in biochemical experiments. Long-range effects of Ca^{2+} binding, ATP binding and phosphorylation, however, can be deduced to cause changes in the overall topology of SERCA.

Currently, there is no high-resolution structure of an ATP-bound SERCA. In a previous study, we reported structural consequences of the binding of a non-hydrolysable ATP analogue, AMP-PNP (adenosine 5′-[β,γ-imido]triphosphate), to SERCA-N (N domain of SERCA) using solution NMR [5]. Chemical-shift changes due to nucleotide binding were observed, following the addition of AMP-PNP, for at least 29 amino acids within a confined area lining the proposed nucleotide-binding region. These results agreed with earlier analyses by site-directed mutagenesis [1,6], as mutation-sensitive residues with respect to ATP binding exhibited a disruption in their signature chemical shifts upon nucleotide addition to the protein sample.

With the aim of gaining insight on the effect(s) of nucleotide binding on the structural and motional behaviour of SERCA-N, we undertook CD, fluorescence spectroscopy and heteronuclear NMR spin-relaxation analyses in order to characterize protein dynamics in the absence and presence of AMP-PNP. The first two methods were used to probe the global effects of nucleotide binding on the structural stability of the protein. Heteronuclear NMR spin-relaxation spectroscopy was employed subsequently to analyse ^{15}N-backbone dynamics of SERCA-N in solution. Characterization of ^{15}N-backbone dynamics was sought to describe, first, the motional properties of SERCA-N and, secondly, the extent to which nucleotide binding changes ^{15}N-backbone

Abbreviations used: AMP-PNP, adenosine 5′-[β,γ-imido]triphosphate; ER, endoplasmic reticulum; N domain, nucleotide-binding domain; NOE, nuclear Over-hauser effect; R_1, longitudinal relaxation rate constant; R_2, transverse relaxation rate constant; S^2, order parameter; SERCA, sarcoplasmic/endoplasmic-reticulum Ca^{2+}-ATPase; SERCA-N, N domain of SERCA; SR, sarcoplasmic reticulum; τ_c, overall molecular correlation time; TM, transmembrane; T_m, melting temperature.

[1] To whom correspondence should be addressed (mikura@uhnres.utoronto.ca).

dynamics. Findings are discussed in light of the known crystal structure of the entire pump in addition to mutagenesis and biochemical data.

EXPERIMENTAL

Protein expression and purification

SERCA-N consists of 244 residues corresponding to the ATP-binding domain of SERCA. Rabbit SERCA1a cDNA coding for Thr^{357}–Leu^{600} was cloned into a pET15b vector (Novagen) downstream of His_6 and thrombin recognition sequences, expressed in *Escherichia coli* strain BL21(DE3), and purified from the soluble extract essentially as described previously [5]. The samples were exchanged into a buffer containing 25 mM potassium phosphate, pH 7.6, 200 mM Na_2SO_4, 300 mM NaCl, 1 mM EDTA and 1 mM TCEP [Tris(2-carboxyethyl)phosphine hydrochloride] with or without a 10× molar excess of AMP-PNP (Sigma).

CD analysis

CD spectra were recorded using an Aviv 62DS spectropolarimeter at 23 °C. All measurements were taken in a quartz cuvette with a 0.1 cm path length. For guanidinium chloride denaturation, protein samples at a concentration of 0.15 mg/ml (5 μM) were used and readings at 222 nm were recorded using a 60 s averaging time. For thermal denaturation, a 0.45 mg/ml (30 μM) sample was used and ellipticity was monitored at 222 nm with a 60 s equilibration time followed by a 10 s averaging period. Each point in the guanidinium chloride melting curve was corrected for background reading using a blank solution consisting of the appropriate concentration of guanidinium chloride.

Tryptophan fluorescence studies

Fluorescence spectra were recorded on a Shimadzu RF-5301 spectrofluorophotometer. Tryptophan fluorescence was determined for the same protein samples used for CD measurements, using an excitation wavelength of 295 nm and monitoring emission between 300 and 450 nm. All readings were corrected for background absorption.

NMR spectroscopy

^{15}N-labelled SERCA-N was prepared as described previously [5]. Two 1.5 mM protein samples in a 92 % ^1H_2O/8 % ^2H_2O-based buffer consisting of 25 mM Tris/HCl, pH 7.6, 200 mM Na_2SO_4, 300 mM NaCl, 10 mM DTT (dithiothreitol) and 10 mM benzamidine were used to measure ^{15}N-backbone relaxation in the absence or presence of 10 mM AMP-PNP. NMR spectroscopy was performed at 296 K on a Varian Inova spectrometer operating at a ^{1}H Larmor frequency of 600.23 MHz. Data sets were processed using NMRPipe and NMRDraw [7].

NMR relaxation measurements

Sensitivity-enhanced protein-detected heteronuclear NMR experiments designed to measure ^{15}N T_1, $T_{1\rho}$, and $\{^1H\}$-^{15}N NOE (nuclear Overhauser effect) were recorded [8,9]. All experiments were performed using spectral widths of 31.3 and 15 p.p.m. in the ^{15}N (F_1) and ^{1}H (F_2) dimensions respectively, acquiring 128×1152 complex points in $F_1 \times F_2$ dimensions. The ^{1}H carrier frequency was set to the frequency of the water resonance (4.79 p.p.m.), and the ^{15}N carrier frequency was set to 116 p.p.m. (nucleotide-free) or 115.56 p.p.m. (nucleotide-bound).

Analysis of relaxation data

^{15}N T_1 values were determined from nine spectra recorded with relaxation-delay times of 10, 150, 310, 490, 680, 900, 1150, 1440 and 1800 ms. ^{15}N $T_{1\rho}$ values were measured from eight spectra recorded with relaxation-delay times of 10, 20, 30, 40, 50, 60, 80 and 100 ms. Peak intensities were obtained using the NMRDraw and SeriesTab software [7]. ^{15}N T_1 and $T_{1\rho}$ values for each residue were obtained by fitting peak intensities to a mono-exponential decay function:

$$I(\mathrm{t}) = I_{\mathrm{o}}{}^{\mathrm{e}-t/T}$$

where I_o is the initial peak intensity, t is the delay time in seconds and T is the relaxation time constant. Relaxation rates R_1 (longitudinal) and $R_{1\rho}$ (transverse) were calculated as the reciprocal values of T_1 and $T_{1\rho}$ respectively. Calculation of R_2 was performed according to the following relationship:

$$R_{1\rho} = R_1 \cdot \cos^2\theta + R_2 \cdot \sin^2\theta,$$

where $\theta = \tan^{-1}(\nu_1/\Delta\nu)$, ν_1 is the spin-lock frequency, $\Delta\nu$ is the difference between ^{15}N offset frequency and the ^{15}N carrier frequency. Spin-lock frequency (ν_1) was 1633.99 Hz for both free and nucleotide-bound samples. Errors in relaxation rates were obtained by Monte Carlo analysis. Steady-state $\{^1H\}$-^{15}N NOE values were determined from the ratio of peak heights with proton saturation to that without proton saturation. Uncertainties in peak heights were given by the S.D. of the background noise in the spectra. Errors in NOE values were obtained by propagating the uncertainties in the peak heights.

ModelFree analysis

Relaxation parameters were used in programs developed by Palmer et al. ([11,12]; http://cpmcnet.columbia.edu/dept/gsas/biochem/labs/palmer/) to analyse ^{15}N-backbone dynamics. Initial values for the overall correlation time (τ_c) were calculated on a per-residue basis from R_2/R_1 ratios, excluding residues with steady-state NOE ratios below 0.70. Data were fitted to an axially-symmetric model, resulting in τ_c values of 22.6 and 22.7 ns for the apo- and the nucleotide-bound protein respectively. ModelFree was used to calculate order parameters (S^2), wherein relaxation data were fitted to three models only: M1 (S^2), M2 (S^2, τ_c), and M3 (S^2, R_{ex}). Model selection criteria used by Mandel et al. [12] were implemented. Values of τ_c were subsequently refined by excluding all residues with $S^2 < 0.75$ or $R_{ex} > 1$ s^{-1}, in addition to the residues with NOE values < 0.70. Optimized τ_c values (see Table 1) were used in another ModelFree run to refine S^2 values.

RESULTS AND DISCUSSION

Effect of nucleotide binding on protein unfolding and stability

SERCA-N is a 28 kDa globular domain of the Ca^{2+}-ATPase which binds ATP, but lacks ATPase activity. The structure of SERCA1a in the Ca^{2+}-bound state revealed that this domain forms an independently folded entity [2]. Our earlier NMR analysis demonstrated that this domain was highly folded in isolation, as indicated by the highly dispersed peak pattern in ^{1}H-^{15}N HSQC (heteronuclear single-quantum coherence) spectra, in both the presence and the absence of AMP-PNP [5]. However, an in-depth understanding of the folding characteristics of SERCA-N has not yet been attained. Far UV CD studies were carried out to assess loss of secondary structure of SERCA-N upon addition of a denaturant, guanidinium chloride, or due to increasing the

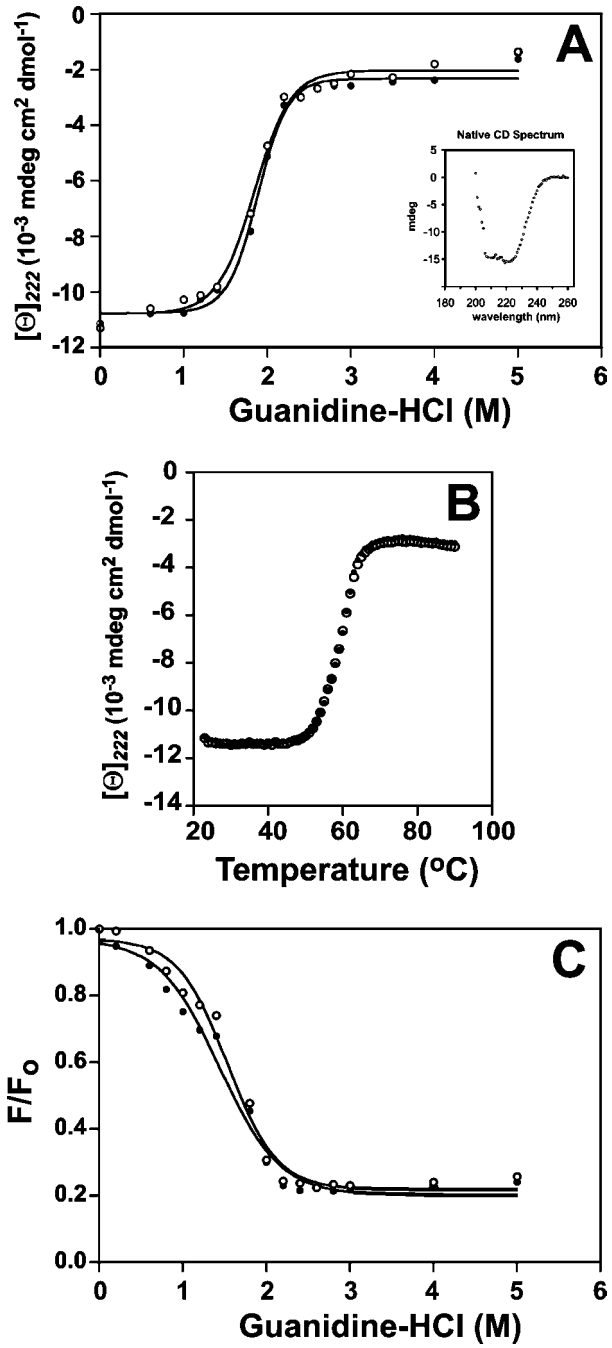

Figure 1 CD and fluorescence studies of SERCA-N

Secondary-structure loss due to protein unfolding by guanidinium chloride (guanidine-HCl) (**A**) and temperature (**B**) was monitored by measuring mean molar ellipticity [Θ] at 222 nm. Tertiary-structure content was probed from tryptophan fluorescence (emission maxima, 338–350 nm) (**C**); normalized fluorescence (F/F_0) is plotted for SERCA-N in the presence of increasing guanidinium chloride concentrations. Open circles (○) indicate apo- protein readings, whereas filled circles (●) indicate measurements from AMP-PNP-bound protein.

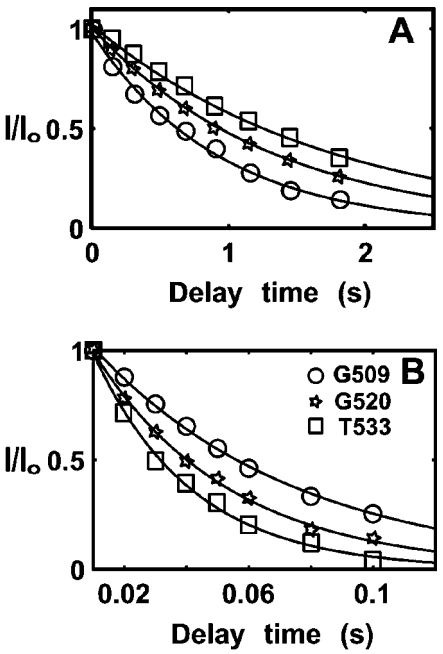

Figure 2 Normalized peak intensities as function of relaxation delay from ^{15}N-relaxation experiments

Representative mono-exponential decay plots due to ^{15}N T_1 (**A**) and ^{15}N T_2 (**B**) relaxation for residues Gly^{509} (G509), Gly^{520} (G520) and Thr^{533} (T533) are shown. R_2 values were characteristically low (i.e. faster transverse relaxation) for residues in mobile loop regions (e.g. Gly^{509}) undergoing nanosecond motions. In contrast, R_1 values were relatively greater for these residues in mobile regions (i.e. slower longitudinal relaxation) relative to residues in more structured and less dynamic parts of the molecule (e.g. Thr^{533}, β10). As an example of mid-range values for R_1 and R_2, the decay curves of Gly^{520} (located in α4) are shown.

temperature. SERCA-N consists of 244 residues, of which 72 (approx. 30%) are located in helical regions and 62 (approx. 25%) are located in β-sheets, based on the available crystal structure data (Protein Data Bank accession numbers 1EUL and 1IWO). The CD spectrum (Figure 1A, inset) is characteristic of the helical content as indicated by the presence of absorption minima at 208 and 222 nm. Guanidinium chloride induced unfolding of apo-SERCA-N in a co-operative manner, manifested by the sharp transition between the folded and unfolded states that is characteristic of globular proteins (Figure 1A). Thermal denaturation was co-operative as well, with a T_m (melting point) value of 59.5 °C (Figure 1B). Because high temperatures resulted in protein precipitation, efforts to refold the thermally denatured protein were unsuccessful. It is noteworthy that protein unfolding, thermally or by guanidinium chloride, gave no evidence to the formation of stable partially unfolded intermediates, as indicated by the absence of a plateau region in the middle of the unfolding curves.

Subsequently, tryptophan fluorescence spectroscopy was employed to probe tertiary-structure perturbation due to denaturation by guanidinium chloride. SERCA-N contains a single tryptophan residue, Trp^{552}, located at the tail-end of a peripheral helix (α5), whose solvent-exposed surface area is 4.7% of the total amino acid area. Emission was monitored at 23 °C for protein samples, whereby maximal signal was obtained at 338 nm, due to the presence of Trp^{552} in a hydrophobic buried region. Protein unfolding due to the addition of increasing amounts of guanidinium chloride was marked by a sharp decline in tryptophan fluorescence emission, indicating an increase in solvent accessibility and loss of tertiary structure (Figure 1C, open circles). A red-shift in emission maximum from 338 nm for the native protein to 345–350 nm for the partially unfolded states (from 1.8 M guanidinium chloride and onward) was observed due to rising exposure to the solvent (results not shown).

We then asked whether nucleotide binding affects the stability or unfolding pattern of SERCA-N. *A priori*, we were interested in two equally valid possibilities with regards to ligand-binding

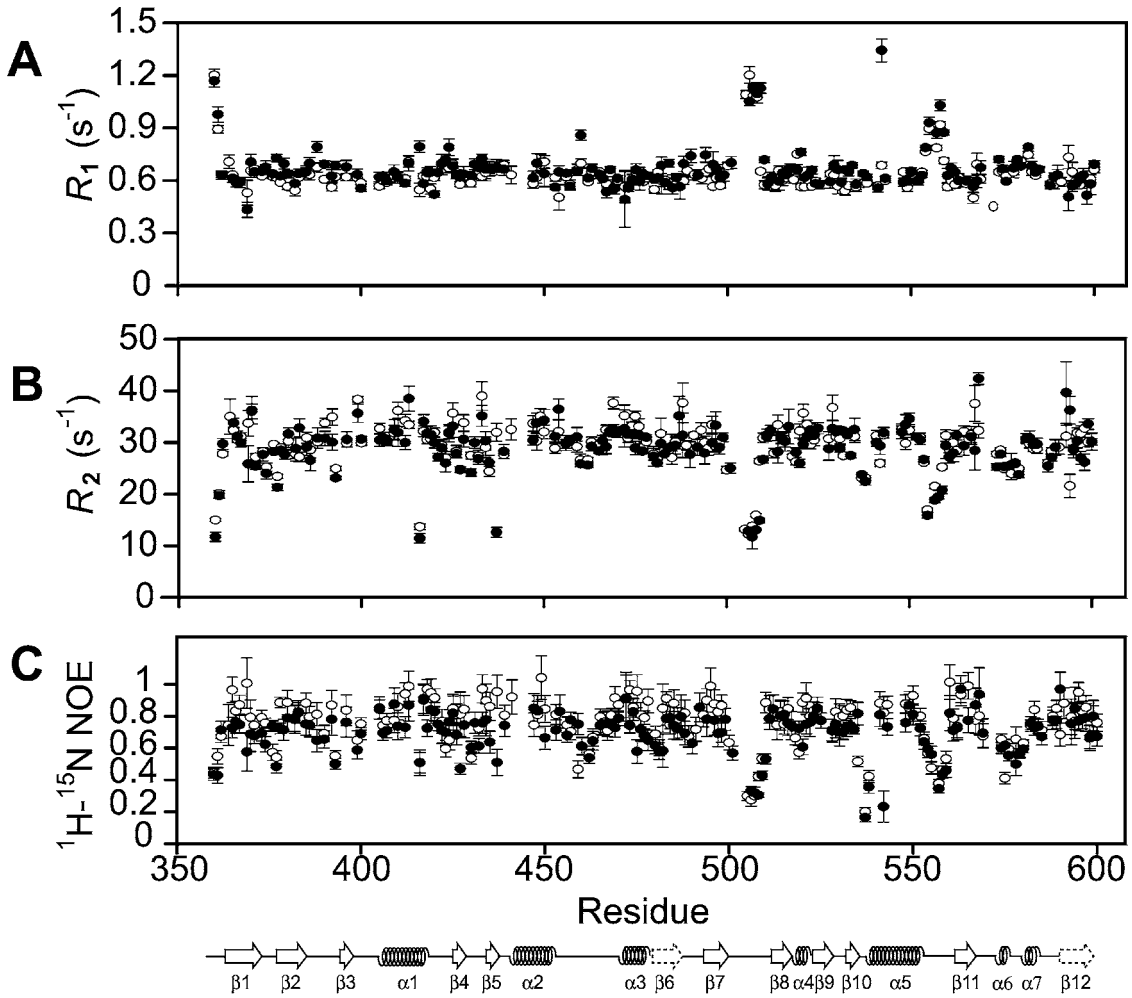

Figure 3 Summary of relaxation parameters of SERCA-N at 600 MHz

Values of ^{15}N R_1 (**A**), ^{15}N R_2 (**B**) and ^{1}H-^{15}N NOE ratios (**C**) are plotted as a function of residue number. Data for apo-SERCA-N are shown as open circles, and that for AMP-PNP-bound SERCA-N are shown as filled circles. Approximate positions of secondary-structure elements are shown at the bottom.

effects: induction of localized conformational changes and/or competition with the unfolding pathway. The unfolding experiments were repeated in the presence of saturating amounts of the nucleotide (10× molar excess). Binding of SERCA-N to the nucleotide ligand did not affect the pattern of protein unfolding significantly, as the unfolding curves were nearly superimposable for the apo- and AMP-PNP-bound forms (Figures 1A–1C, filled circles).

The findings of the CD and fluorescence analyses are consistent with each other, indicating that, first, protein unfolding is highly co-operative; secondly, the absence of stable partially unfolded intermediates; and, thirdly, substrate binding does not impart significant protection from denaturation. Thus binding of the nucleotide ligand to SERCA-N does not alter the global properties of unfolding or protein stability in a profound manner. This can be rationalized by the relatively weak binding constant (k_d, ~0.7 mM [13] or ~2.4 mM, according to NMR titration data) for the nucleotide. Such weak binding may not introduce the additional forces necessary to stabilize the bound state to the extent that it could be detected by CD or tryptophan fluorescence. Furthermore, these results indicate that the ligand induces limited global conformational rearrangement/perturbation. Indeed, this is consistent with our previous NMR titration data where the ^{1}H-^{15}N chemical shifts of a small number of residues (29 out of 244) confined to one region were affected due to ligand binding [5].

Furthermore, limitations inherent in the CD and tryptophan fluorescence analyses preclude an unequivocal conclusion on the lack of any conformational changes, especially small-magnitude changes. This is because CD studies detect, mainly, changes in secondary structure, but are insensitive to changes in random-coil regions that might make some contacts with the ligand. Similarly, tryptophan fluorescence data were not conclusive. Fast quenching of fluorescence emission from the single tryptophan residue present in the protein due to unfolding might mask small localized changes that occur at the ATP-binding cavity. Thus further detailed analysis was necessary to detect and describe, in quantitative terms, minimal conformational changes that might occur upon binding.

Backbone dynamics of SERCA-N

We chose to employ ^{15}N-backbone-relaxation measurements in order to analyse the conformational dynamics of SERCA-N in solution and to dissect site-specific changes upon nucleotide binding. This method is very reliable in assessing picosecond–nanosecond time-scale conformational changes [14,15].

Table 1 Mean values of relaxation and S^2

Parameter	Free SERCA-N	Nucleotide-bound SERCA-N
^{15}N R_1 (s^{-1})	0.642 ± 0.023	0.668 ± 0.030
^{15}N R_2 (s^{-1})	29.397 ± 1.064	28.809 ± 1.335
^{1}H-^{15}N NOE	0.763 ± 0.067	0.698 ± 0.066
τ_c* (ns)	22.37 ± 0.05	22.21 ± 0.07
S^2	0.927 ± 0.056	0.867 ± 0.057

* τ_c is defined as the time required for the molecule to rotate about its principal axis by 1 radian.

Table 2 Motional models selected for SERCA-N residues in model-free analysis

Model	Free SERCA-N	Nucleotide-bound SERCA-N
M1*	117	108
M2†	30	35
M3‡	2	2
None	17	21
Total	166	166

* Model parameter: S^2
† Model parameters: S^2 and τ_e
‡ Model parameters: S^2 and R_{ex}

Values of R_1 and R_2 were calculated by least-squares fitting of the decay in peak heights over the time-delay period into a mono-exponential function (Figure 2). Relaxation data could not be determined for all of the 238 non-proline residues, mainly due to spectral overlap. Relaxation data are reported for 166 residues, representing approx. 70 % of available peaks (Figure 3). It is noted that residues at the N-terminus and those in some surface loop regions (L1, 501–510; L2, 553–559) exhibited low NOE and R_2 values, as expected for regions undergoing fast internal motions. Indeed, these regions exhibited the largest deviation from the mean values of the measured relaxation parameters (Table 1). This was observed for both apo- and nucleotide-bound SERCA-N, indicating inherent structural mobility regardless of binding state.

To investigate fast time-scale dynamics in SERCA-N, ModelFree analysis [11,12] was employed to calculate S^2 for the N-H_N backbone vectors of SERCA-N in the presence and absence of AMP-PNP (Figure 4). Table 2 summarizes the various motional models that were implemented in the ModelFree analysis. For most residues, the simplest models (M1 and M2) were sufficient to describe internal dynamics. Some residues could not be fitted

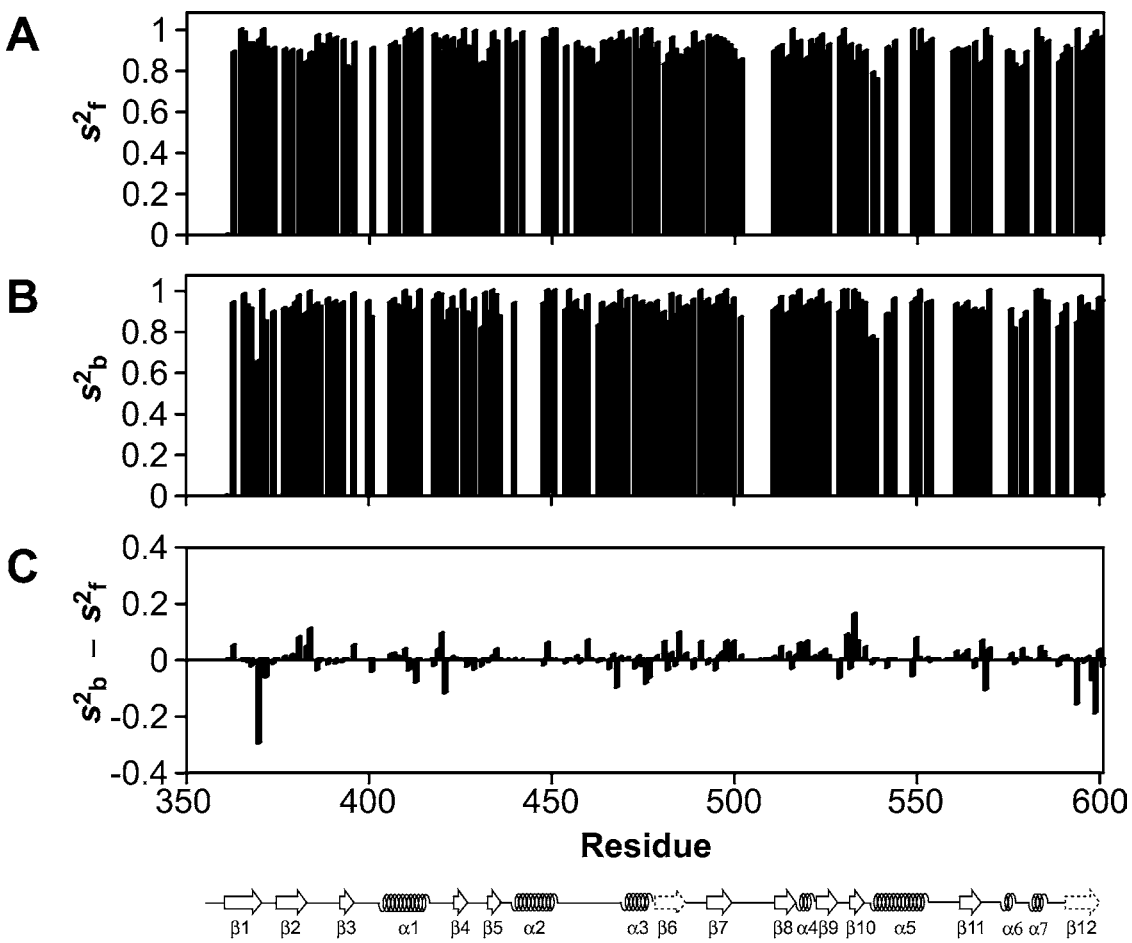

Figure 4 Backbone amide S^2

S^2 were calculated for the apo-SERCA-N (**A**) (S^2f), and in the presence of AMP-PNP (**B**) (S^2b). Differences in S^2 values are plotted (**C**). Positions of secondary-structure elements are shown at the bottom.

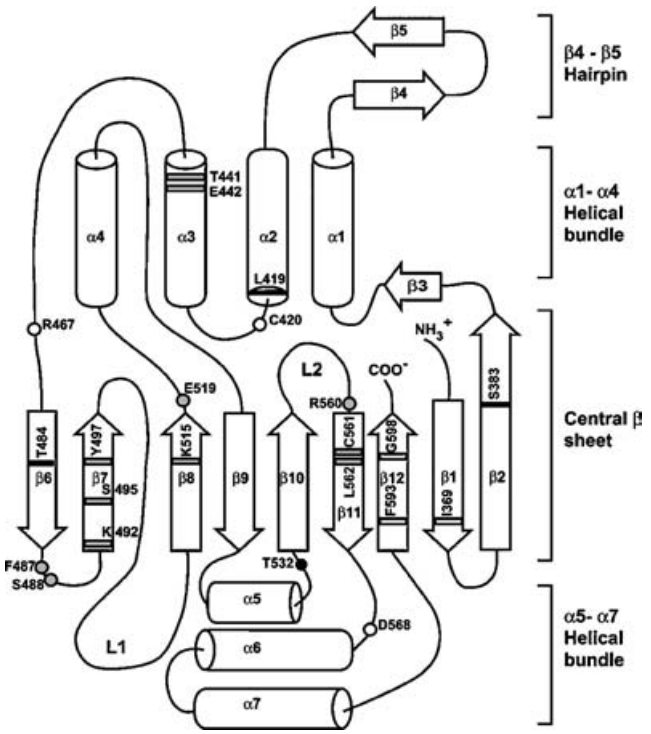

Figure 5 A schematic representation of the topology of SERCA-N

Helical segments are depicted by cylinders and β-strands are indicated by arrows. The relative positions of some residues involved in nucleotide binding are shown in grey. Residues for which there is an increase or decrease in backbone ^{15}N mobility are shown in white and black respectively.

into any of the three models, such as residues in surface loops L1 (501–510) and L2 (553–559), and the N-terminal residues, due to the complexity of dynamics of these regions. Nonetheless, the order parameter data indicated that most of the backbone residues of SERCA-N were remarkably rigid, with 75 % of residues fitted in motional models having S^2 values > 0.9 (Figures 4A and 4B).

A comparative analysis of the values of order parameters of apo- and AMP-PNP-bound SERCA-N was performed to infer local effects of ligand binding on backbone dynamics. As illustrated in Figure 4(C), most residues of SERCA-N exhibited S^2 differences below the chosen significance cut-off level ($\Delta S^2 = 0.09$). Significant differences in S^2 values were found for ten residues (see Figure 5): six were differences that enhanced backbone internal mobility (negative differences: Ile^{369}, Cys^{420}, Arg^{467}, Asp^{568}, Phe^{593} and Gly^{598}), while four differences introduced more rigidity to the backbone (positive differences: Ser^{383}, Leu^{419}, Thr^{484} and Thr^{532}).

These results indicate that nucleotide binding introduced both rigidity and flexibility on different parts of the backbone of SERCA-N. Such diverse effects of binding have been reported for other protein–ligand complexes [16,17].

Correlation with biochemical data

In order to gain a better understanding of our NMR findings in conjunction with the available biochemical data on ATP-binding, a structural model of nucleotide binding to SERCA-N was sought. In the absence of co-ordinates for the nucleotide–SERCA complex, we carried out a modelling study of ATP binding to SERCA-N. This was based, primarily, on our previously published NMR data concerning binding residues [5], with additional constraints supplied from recent site-directed mutagenesis [18,19] and biophysical [20,21] data. Modelling was performed manually at the beginning by docking ATP into SERCA-N (partial co-ordinates from Protein Data Bank accession number 1IWO; residues 357–600). The energy of the SERCA-N–ATP complex was then minimized using CNS [22]. Figure 6 illustrates our model of the ATP-bound SERCA-N complex.

In Figure 5, a simplified topology diagram of SERCA-N displays the relative positions of residues which contribute most significantly to nucleotide binding (grey) as well as residues whose backbone S^2 values vary significantly due to binding (black and white). Interestingly, most of the latter group of residues are located in or near the central β-sheet domain, and in close proximity to most of the nucleotide-binding residues (Figures 5 and 6B). This central β-sheet forms the scaffold of the protein, where it is surrounded by the two helical bundles. The convergence of residues exhibiting significant ΔS^2 values due to nucleotide binding with many of the ATP-binding residues in this location highlights the role of the central β-sheet in relation to its interactions with the nucleotide. Yet, with the exception of Leu^{419} and Cys^{420}, there is no reported evidence of a direct role for residues exhibiting significant ΔS^2 values in nucleotide binding. The residues which are involved directly in nucleotide binding and for which relaxation data was available (e.g. Ser^{488}, Lys^{492}, Lys^{515}, Glu^{519}, Arg^{560} and Leu^{562}) did not display significant ΔS^2 values. The observed changes in S^2 values must, therefore, account for indirect roles of residues outside of the nucleotide-binding core.

Two sites with significant ΔS^2 are found at Leu^{419} and Cys^{420} (Figures 5 and 6A). From previous NMR titration data [5], there was evidence that the L^{419}CNDS^{423} loop (α2–α3 loop; Figure 5) lies on the upper periphery of the nucleotide-binding pocket. It is of interest that the binding of AMP-PNP has opposite effects on the backbone of two consecutive residues, Leu^{419} and Cys^{420}, with the latter becoming more flexible and the former becoming more rigid. Such localized changes in the dynamics of the α2–α3 loop region upon binding are indication of substrate-induced modifications, albeit small. The rigidifying effect of nucleotide binding at Leu^{419} appears to be counterbalanced by increasing flexibility at Cys^{420}, perhaps as a means to compensate for entropic loss.

Other sites of significant changes to the S^2 values are Ile^{369} and Phe^{593}, where there is a concerted decrease in S^2 values upon AMP-PNP binding. In the crystal structure, the side chains of Ile^{369} (β1) and Phe^{593} (β12) lie in close proximity to one another and are involved in hydrophobic interactions. A concurrent change in the ^{15}N-backbone dynamics at these neighbouring sites indicates that their mobilities are correlated. It suggests that there is a small change in the conformation of the corresponding β-strands (Figure 5), leading to disruption of their packing interactions at one end where Ile^{369} and Phe^{595} are located. Interestingly, these sites are approx. 16 Å (where 1 Å = 0.1 nm) apart from the nearest residue in the nucleotide-binding region (Phe^{487}) and therefore account for long-range effects of nucleotide binding.

The observed increase in backbone mobility of Gly^{598} (β12) can be explained similarly by disruption of interactions with Cys^{561} and/or Leu^{562} located at β11 (Figure 5). Both Cys^{561} and Leu^{562} play an important role in binding to the nucleotide, as evidenced by NMR data [5]. Recent mutagenesis studies on SERCA1a confirmed the importance of the side chain of Leu^{562} in nucleotide binding [18]. The side chain of Cys^{561} does not seem to play a direct role in binding, as replacing it with tryptophan did not alter the k_d for ATP. Therefore, based on our NMR data, main-chain interactions of Cys^{561} with AMP-PNP accounts for the observed chemical shift changes in the amide-N position of Cys^{561}. Accordingly, the observed increase of backbone

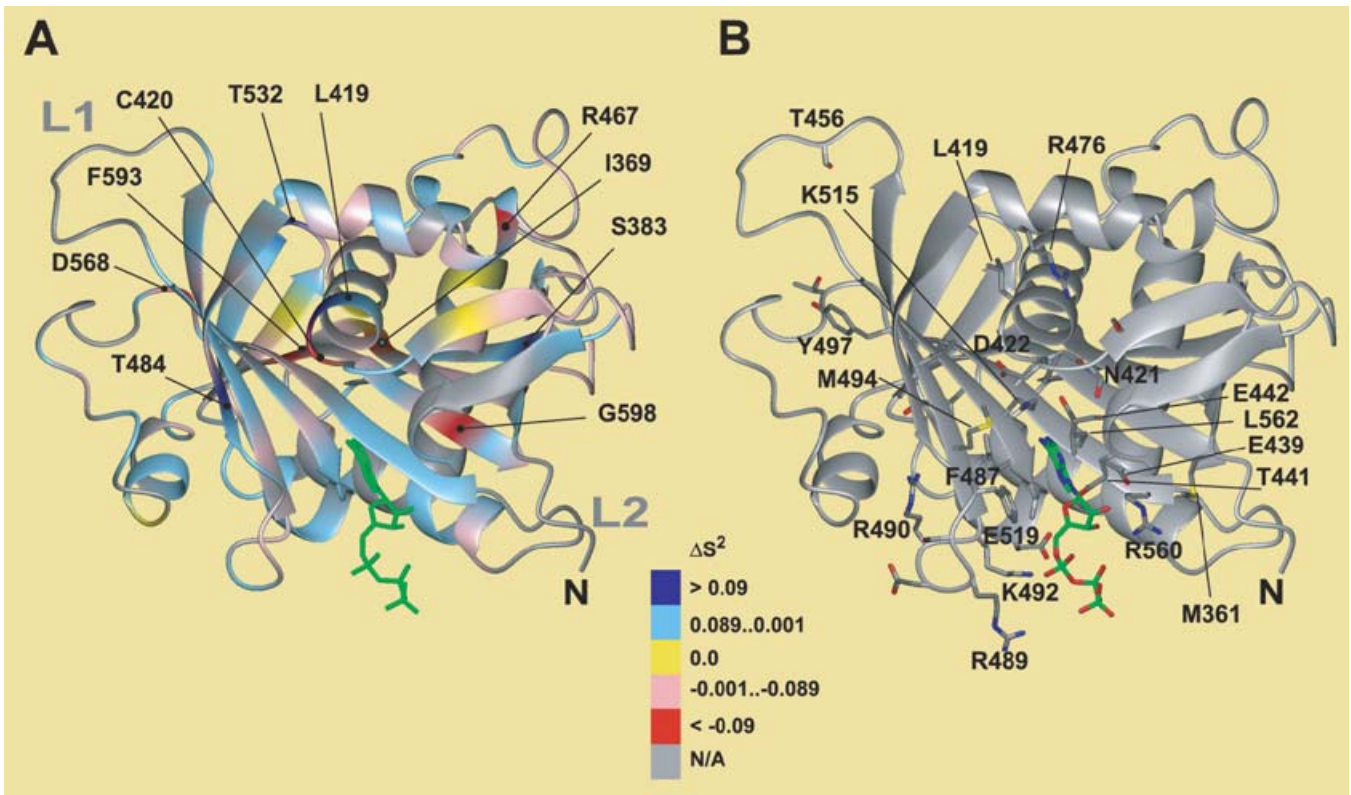

Figure 6 Mapping ΔS^2 values on a structural model of the ATP-bound SERCA-N

The co-ordinates of SERCA-N, derived from the crystal structure of the Ca^{2+}-ATPase in the E2 conformation (Protein Data Bank accession number 1IWO; residues 357–600) were used to model the position of ATP in the putative binding pocket based on NMR, mutagenesis and biophysical data (see the Discussion). (**A**) Differences in ^{15}N-backbone order parameters (ΔS^2) between the nucleotide-bound and apo-SERCA-N are mapped and colour-coded, according to the sign and significance of ΔS^2 values. Residues with significant positive differences are shown in dark blue; those with significant negative differences shown in red; non-significant positive and negative ΔS^2 values are shown in light blue and pale pink respectively. Zero ΔS^2 values (no change) are shown in yellow. Residues which could not be fitted in any motional model or for which no relaxation data were available are coloured grey. (**B**) Side chains of residues that are important for binding, as identified by NMR titration with AMP-PNP and mutagenesis studies are shown. This diagram was generated using MOLMOL [24].

mobility at Gly^{598} can be explained as an indirect consequence of interaction of the nucleotide with neighbouring Leu^{562} and Cys^{560}. It is plausible that occupation of the binding cavity by the nucleotide, and the subsequent formation of hydrogen bonding and hydrophobic interactions with neighbouring residue such as Cys^{561} and Leu^{562} had the effect of displacing inter-strand hydrogen-bonding contacts with Gly^{598}. This, coupled with the proximity of Gly^{598} to the C-terminus and the inherent flexibility of the last part of $\beta 12$ in solution [5], offers explanation as to the observed decrease in backbone S^2 value in the presence of AMP-PNP. It is noteworthy that nucleotide binding had no significant effects on the backbone dynamics of either Cys^{651} or Ile^{562}, as their S^2 values remained high.

Enhancement of backbone rigidity has been observed at Thr^{484} ($\beta 6$). This can be explained by proximity to Phe^{487}, which is important for ring-stacking interactions with the adenine moiety of the nucleotide [5,23]. There is NMR evidence for distortion of $\beta 6$ in the absence of nucleotide, as indicated by an early chemical-shift index study [5] and low NOE values reported in the present study. Restriction of backbone mobility at Thr^{484} upon nucleotide binding is, therefore, considered significant. Interestingly, Ser^{495} and Tyr^{497}, on the opposite β strand ($\beta 7$), are within hydrogen-bonding distance of Thr^{484}. Both Ser^{495} and Tyr^{497} are located in a stretch of $\beta 7$ ($M^{494}SVY^{497}$) that has been reported to be affected by nucleotide binding, as evidenced by changes in ^1H-^{15}N chemical shift values upon titration with AMP-PNP [5]. Thus binding of AMP-PNP appears to reduce backbone disorder at Thr^{484}, perhaps allowing better interaction with Ser^{495} and/or Tyr^{497}. This would, in effect, strengthen inter-strand interactions between $\beta 6$ and $\beta 7$, and possibly enhance interaction of the aromatic ring Phe^{487} with the purine moiety of the nucleotide.

Other sites where a change in backbone mobility was observed (Arg^{467}, Asp^{568}, Ser^{383}, Thr^{532} and Asp^{568}) cannot be explained currently, due to lack of mutagenesis data and detachment from the nucleotide-binding core.

The above findings strongly indicate that conformational changes occurring in SERCA at different reactive stages, as evidenced by altered cytoplasmic domain topologies, involve movement of SERCA-N as a rigid body. Movement of SERCA-N would be requisite for the phosphorylation of Asp^{351} by ATP, thus driving further conformational changes leading to translocation of Ca^{2+} across the SR/ER membrane.

Concluding remarks

Previous NMR data on apo-SERCA-N indicated that this state is folded, but no information was available on conformational stability and dynamics. The present CD and fluorescence data clearly demonstrate that (i) SERCA-N is highly stable (T_m, 59.5 °C) in both the absence and presence of AMP-PNP; (ii) denaturation is highly co-operative and does not involve formation of stable partially unfolded intermediates; and (iii) AMP-PNP does

not alter the global unfolding properties of SERCA-N. These results indicate that SERCA-N can exist as a single structural entity, even in the apo state, with markedly ordered structural characteristics which are consistent with the highly globular α/β structure. ^{15}N-relaxation studies on SERCA-N revealed that AMP-PNP binding has internally counterbalancing effects on the structural flexibility of the backbone that propagate through the central β-sheet domain. Both rigidifying and mobility-enhancement effects were observed. Such effects were either in a direct manner around the nucleotide-binding core (e.g. Ile^{419} and Cys^{420}) or through long-range interactions (e.g. Ile^{369}/Phe^{593}, Thr^{484} and Gly^{593}). Overall, most residues in the binding core retained backbone rigidity after binding to AMP-PNP. These results suggest the presence of a fine balance between rigidifying effects upon nucleotide binding and minimization of overall entropic loss.

We thank Dr Tapas Mal and Dr Ahmed Khorchid from the lab of M. I. for assistance with NMR data collection and help with CD measurements respectively. The technical help of Dr Ranjith Muhandiram from the NMR centre is especially appreciated. This research was supported by grants to D. H. M. from the Canadian Institutes of Health Research (CIHR) and the Heart and Stroke Foundation of Canada (HSFC), and to M. I. from the HSFC. M. I. is a CIHR Senior Investigator. M. A. received a doctoral award from the HSFC.

REFERENCES

1 MacLennan, D. H., Rice, W. J. and Green, N. M. (1997) The mechanism of Ca^{2+} transport by sarco(endo)plasmic reticulum Ca^{2+}-ATPases. J. Biol. Chem. **272**, 28815–28818
2 Toyoshima, C., Nakasako, M., Nomura, H. and Ogawa, H. (2000) Crystal structure of the calcium pump of sarcoplasmic reticulum at 2.6 Å resolution. Nature (London) **405**, 647–655
3 Stokes, D. L., Zhang, P., Toyoshima, C., Yonekura, K., Ogawa, H., Lewis, M. R. and Shi, D. (1998) Cryoelectron microscopy of the calcium pump from sarcoplasmic reticulum: two crystal forms reveal two different conformations. Acta Physiol. Scand. Suppl. **643**, 35–43
4 Toyoshima, C. and Nomura, H. (2002) Structural changes in the calcium pump accompanying the dissociation of calcium. Nature (London) **418**, 605–611
5 Abu-Abed, M., Mal, T. K., Kainosho, M., MacLennan, D. H. and Ikura, M. (2002) Characterization of ATP-binding domain of the sarco(endo)plasmic reticulum Ca^{2+}-ATPase: probing nucleotide binding by multidimensional NMR. Biochemistry **41**, 1156–1164
6 Wuytack, F., Raeymaekers, L. and Missiaen, L. (2002) Molecular physiology of the SERCA and SPCA pumps. Cell Calcium **32**, 279–305
7 Delaglio, F., Grzesiek, S., Vuister, G. W., Zhu, G., Pfeifer, J. and Bax, A. (1995) NMRPipe: a multidimensional spectral processing system based on UNIX pipes. J. Biomol. NMR **6**, 277–293
8 Farrow, N. A., Muhandiram, R., Singer, A. U., Pascal, S. M., Kay, C. M., Gish, G., Shoelson, S. E., Pawson, T., Forman-Kay, J. D. and Kay, L. E. (1994) Backbone dynamics of a free and phosphopeptide-complexed Src homology 2 domain studied by ^{15}N NMR relaxation. Biochemistry **33**, 5984–6003
9 Akke, M. and Palmer, 3rd, A. G. (1996) Monitoring macromolecular motions on microsecond to millisecond time scales by R1rho-R1 constant relaxation time NMR spectroscopy. J. Am. Chem. Soc. **118**, 911–912
10 Reference deleted
11 Palmer, 3rd, A. G., Rance, M. and Wright, P. E. (1991) Intramolecular motions of a zinc finger DNA-binding domain from XFIN characterized by proton-detected natural abundance C^{12} heteronuclear NMR spectroscopy. J. Am. Chem. Soc. **113**, 4371–4380
12 Mandel, A. M., Akke, M. and Palmer, 3rd, A. G. (1996) Dynamics of ribonuclease H: temperature dependence of motions on multiple time scales. Biochemistry **35**, 16009–16023
13 Champeil, P., Menguy, T., Soulie, S., Juul, B., de Gracia, A. G., Rusconi, F., Falson, P., Denoroy, L., Henao, F., le Maire, M. and Moller, J. V. (1998) Characterization of a protease-resistant domain of the cytosolic portion of sarcoplasmic reticulum Ca^{2+}-ATPase: nucleotide- and metal-binding sites. J. Biol. Chem. **273**, 6619–6631
14 Akke, M. (2002) NMR methods for characterizing microsecond to millisecond dynamics in recognition and catalysis. Curr. Opin. Struct. Biol. **12**, 642–647
15 Palmer, 3rd, A. G. (2001) NMR probes of molecular dynamics: overview and comparison with other techniques. Annu. Rev. Biophys. Biomol. Struct. **30**, 129–155
16 Finerty, Jr, P. J., Muhandiram, R. and Forman-Kay, J. D. (2002) Side-chain dynamics of the SAP SH2 domain correlate with a binding hot spot and a region with conformational plasticity. J. Mol. Biol. **322**, 605–620
17 Mittermaier, A., Varani, L., Muhandiram, D. R., Kay, L. E. and Varani, G. (1999) Changes in side-chain and backbone dynamics identify determinants of specificity in RNA recognition by human U1A protein. J. Mol. Biol. **294**, 967–979
18 Clausen, J. D., McIntosh, D. B., Vilsen, B., Wooley, D. G. and Andersen, J. P. (2003) Importance of conserved N-domain residues Thr^{441}, Glu^{442}, Lys^{515}, Arg^{560} and Leu^{562} of sarcoplasmic reticulum Ca^{2+}-ATPase for MgATP binding and subsequent catalytic steps. J. Biol. Chem. **278**, 20245–20258
19 Ma, H., Inesi, G. and Toyoshima, C. (2003) Substrate-induced conformational fit and headpiece closure in the Ca^{2+}-ATPase (SERCA). J. Biol. Chem. **278**, 28938–28943
20 Liu, M. and Barth, A. (2003) Mapping interactions between the Ca^{2+}-ATPase and its substrate ATP with infrared spectroscopy. J. Biol. Chem. **278**, 10112–10118
21 Liu, M. and Barth, A. (2003) TNP-PNP binding to the sarcoplasmic reticulum Ca^{2+}-ATPase studied by infrared spectroscopy. Biophys. J. **85**, 3262–3270
22 Brunger, A. T., Adams, P. D., Clore, G. M., DeLano, W. L., Gros, P., Grosse-Kunstleve, R. W., Jiang, J. S., Kuszewski, J., Nilges, M., Pannu, N. S. et al. (1998) Crystallography and NMR system (CNS): a new software system for macromolecular structure determination. Acta Crystallogr. D Biol. Crystallogr. **54**, 905–921
23 Hofbauerova, K., Kopecky, V., Ettrich, R., Kubala, M., Teisinger, J. and Amler, E. (2003) ATP-binding is stabilized by a stacking interaction within the binding site of Na^+/K^+-ATPase. Biochem. Biophys. Res. Commun. **306**, 416–420
24 Koradi, R., Billeter, M. and Wüthrich, K. (1996) MOLMOL: a program for display and analysis of macromolecular structures. J. Mol. Graph. **14**, 51–55

Received 29 January 2004/19 February 2004; accepted 25 February 2004
Published as BJ Immediate Publication 26 February 2004, DOI 10.1042/BJ20040168